Soliton squeezing in a highly transmissive nonlinear optical loop mirror

Dmitry Levandovsky, Michael Vasilyev, and Prem Kumar

Department of Electrical and Computer Engineering, Northwestern University, Evanston, Illinois 60208-3118

A perturbation approach is used to study the quantum noise of optical solitons in an asymmetric fiber Sagnac interferometer (a highly transmissive nonlinear optical loop mirror). Analytical expressions for the three second-order quadrature correlators are derived and used to predict the amount of detectable amplitude squeezing along with the optimum power-splitting ratio of the Sagnac interferometer. We find that it is the number-phase correlation owing to the Kerr nonlinearity that is primarily responsible for the observable noise reduction. The group-velocity dispersion affecting the field in the nonsoliton arm of the fiber interferometer is shown to limit the minimum achievable Fano factor. © 1999 Optical Society of America

OCIS codes: 270.6570, 060.5530.

Recently, generation of sub-Poissonian light in an asymmetric fiber Sagnac interferometer was predicted[1] by use of a numerical technique that relies on a positive-P representation.[2] Two groups have validated this prediction,[3,4] demonstrating 3.9 and 5.7 dB of amplitude squeezing, respectively. In this Letter we clarify the physical mechanism that is responsible for this noise reduction by deriving an analytical solution that is based on a perturbation approach.[5,6] We find that the observable amplitude squeezing in the asymmetric Sagnac loop is mainly determined by the strong number-phase correlation, which grows with propagation distance, similar to the cw case studied by Kitagawa and Yamamoto.[7] This squeezing mechanism differs from that of soliton spectral filtering, wherein the noise reduction results mostly from the correlation between the photon number and the bandwidth, which does not grow with distance.[6] We calculate the amount of available squeezing as well as the optimum power-splitting ratio of the Sagnac interferometer and explain the role of the group-velocity dispersion. Our model takes into account the complete contribution of the continuum to the detected quantum noise.[6]

We analyze the following experimental configuration. A short optical pulse is launched into a fiber Sagnac interferometer. The action of the beam splitter results in two independent modes, an $N = 1$ soliton $\hat{a}_{\mathrm{sol}}$ propagating in one direction around the fiber loop and a weaker ($N^2 \ll 1$) dispersive pulse $\hat{a}_{\mathrm{gvd}}$ propagating in the other direction. After propagation around the fiber loop, the two pulses interfere at the same beam splitter, so most of the soliton power appears in the transmitting arm of the interferometer, mixed with a small fraction of the power of the dispersive pulse. The transmitted pulse is subsequently directed onto a photon-counting detector. For a beam splitter with intensity transmission coefficient T the two counterpropagating waves inside the Sagnac loop are $\hat{a}_{\mathrm{sol}}(\xi) = [a_0 + \Delta\hat{a}_{\mathrm{sol}}(\xi)]\exp(i\xi/2)$ and $\hat{a}_{\mathrm{gvd}}(\xi) = i[(1 - T)/T]^{1/2}a_0\exp(-i\psi) + i\Delta\hat{a}_{\mathrm{gvd}}(\xi)$. Here $a_0(\omega) = \pi\,\mathrm{sech}(\pi\omega/2)$ is the fundamental soli-

ton shape in the frequency domain, ξ is the normalized propagation distance inside the loop in units of dispersion length, $\psi \equiv \omega^2\xi/2$ is the quadratic phase shift that is due to the group-velocity dispersion, and $\Delta\hat{a}_{\mathrm{sol}}$ and $\Delta\hat{a}_{\mathrm{gvd}}$ are quantum noises associated with the soliton and the dispersive pulse, respectively, i.e., $[\Delta\hat{a}_i(\omega, \xi), \Delta\hat{a}_j^\dagger(\omega', \xi)] = 2\pi\delta(\omega - \omega')\delta_{ij}$ for $i, j \in \{\mathrm{sol}, \mathrm{gvd}\}$. The two noise operators represent independent coherent states immediately after the beam splitter (at $\xi = 0$): $\langle\Delta\hat{a}_i(\omega, 0)\Delta\hat{a}_j(\omega', 0)\rangle = 0$. In our analysis we consider T to be large enough that the nonlinear effects in the propagation of the weaker pulse $\hat{a}_{\mathrm{gvd}}$ can be neglected, i.e., $\Delta\hat{a}_{\mathrm{gvd}}(\xi)$ remains in a coherent state for all ξ. The soliton $\hat{a}_{\mathrm{sol}}(\xi)$, however, evolves toward a nonclassical state, according to the nonlinear Schrödinger equation.[5,6]

The output field in the transmitting arm of the interferometer is given by

$$\hat{a}_{\mathrm{out}} \equiv a_{\mathrm{out}} + \Delta\hat{a}_{\mathrm{out}} = \sqrt{T}\,\hat{a}_{\mathrm{sol}}(\xi) + i\sqrt{1 - T}\,\hat{a}_{\mathrm{gvd}}(\xi),$$

$$(1)$$

where

$$a_{\mathrm{out}} = \sqrt{T}\,a_0\exp(i\xi/2)\left\{1 - \frac{1 - T}{T}\exp[-i(\psi + \xi/2)]\right\},$$

$$(2)$$

$$\Delta\hat{a}_{\mathrm{out}} = \sqrt{T}\,\Delta\hat{a}_{\mathrm{sol}}(\xi)\exp(i\xi/2) - \sqrt{1 - T}\,\Delta\hat{a}_{\mathrm{gvd}}(\xi). \quad (3)$$

Defining the two noise operators $\Delta\hat{a}_{\mathrm{sol}}^c(\omega, \xi) \equiv [\Delta\hat{a}_{\mathrm{sol}}(\omega, \xi) + \Delta\hat{a}_{\mathrm{sol}}^\dagger(\omega, \xi)]/2$ and $\Delta\hat{a}_{\mathrm{sol}}^s(\omega, \xi) \equiv [\Delta\hat{a}_{\mathrm{sol}}(\omega, \xi) - \Delta\hat{a}_{\mathrm{sol}}^\dagger(\omega, \xi)]/2$, which represent amplitude (cosine) and phase (sine) fluctuations of the soliton field, and using Eqs. (2) and (3), we find the following Fano factor for ideal direct detection (unit detection efficiency) at the transmitting output port:

$$F(\xi) = 1 + T\left(\int |a_{\mathrm{out}}|^2\mathrm{d}\omega/2\pi\right)^{-1}\iint |a_{\mathrm{out}}||a_{\mathrm{out}}'|$$

$$\times \sum_{i, j = \{c, s\}} \Phi^i G_N^{ij}(\omega, \omega', \xi)\Phi^{j'}\mathrm{d}\omega\mathrm{d}\omega'/4\pi^2, \quad (4)$$

where $\Phi^c = \cos\varphi(\omega)$, $\Phi^s = -i\sin\varphi(\omega)$, and $\varphi(\omega) = \arg[a_{\text{out}}(\omega)] - \xi/2$. Our conventions throughout this Letter are to use prime symbols to denote functions of ω', where applicable, and to assume all integrals to be from minus infinity to plus infinity. In Eq. (4) $G_N^{ij}(\omega, \omega', \xi)$ are the normally ordered correlators, which are evaluated at length ξ as

$$G_N^{cc}(\omega, \omega', \xi) \equiv 4\langle: \Delta\hat{a}_{\text{sol}}^c \Delta\hat{a}_{\text{sol}}^{c\prime} :\rangle_\xi, \tag{5}$$

$$G_N^{ss}(\omega, \omega', \xi) \equiv 4\langle: \Delta\hat{a}_{\text{sol}}^s \Delta\hat{a}_{\text{sol}}^{s\prime} :\rangle_\xi, \tag{6}$$

$$G_N^{cs}(\omega, \omega', \xi) \equiv 4\langle: \Delta\hat{a}_{\text{sol}}^c \Delta\hat{a}_{\text{sol}}^{s\prime} :\rangle_\xi$$
$$= -G_N^{cs*}(\omega, \omega', \xi) = G_N^{sc}(\omega', \omega, \xi). \tag{7}$$

We can easily obtain these noise correlators by following the perturbation approach described in Ref. 6. For the sake of convenience we first evaluate them in the time domain and then use the Fourier-transform relation to convert them to the form given in Eqs. (5)–(7). The cosine and sine noise operators in the time domain can be constructed with the normal-mode expansion as follows:

$$[\Delta\hat{a}_{\text{sol}}(\tau, \xi) + \Delta\hat{a}_{\text{sol}}^\dagger(-\tau, \xi)]/2 = \sum_{i=n,p,c} \Delta\hat{X}_i, \tag{8}$$

$$[\Delta\hat{a}_{\text{sol}}(\tau, \xi) - \Delta\hat{a}_{\text{sol}}^\dagger(-\tau, \xi)]/2 = \sum_{i=\theta,\tau,s} \Delta\hat{X}_i, \tag{9}$$

where the six contributing terms are given by $\Delta\hat{X}_{i\in\{n,p,\theta,\tau\}}(\tau, \xi) \equiv \hat{V}_i(\xi)f_i(\tau)$ and $\Delta\hat{X}_{i\in\{c,s\}}(\tau, \xi) \equiv \int \hat{V}_i(\Omega, \xi)f_i(\Omega, \tau)d\Omega/2\pi$. The time-domain normal modes used in the expansion of the cosine operator, $f_n(\tau) = [1 - \tau\tanh(\tau)]\text{sech}(\tau)$, $f_p(\tau) = -i\tau\,\text{sech}(\tau)$, and $f_c(\tau) = \{[(\Omega^2 - 1) - 2i\Omega\tanh(\tau)]\exp(-i\Omega\tau) + 2\,\text{sech}^2(\tau)\cos(\Omega\tau)\}/(\Omega^2 + 1)$, have real Fourier transforms, whereas the modes that are pertinent to the sine operator, $f_\theta(\tau) = -i\,\text{sech}(\tau)$, $f_\tau(\tau) = \tanh(\tau)\text{sech}(\tau)$, and $f_s(\tau) = i\{[(\Omega^2 - 1) - 2i\Omega\tanh(\tau)]\exp(-i\Omega\tau) - 2i\,\text{sech}^2(\tau)\sin(\Omega\tau)\}/(\Omega^2 + 1)$, have imaginary Fourier transforms. Note that we employ the Heisenberg picture, where all the ξ dependence is in the operator coefficients $\hat{V}_i(\xi)$, which are Hermitian and can be associated with either the time- or frequency-dependent modes. Physically, f_n, f_θ, f_p, and f_τ represent perturbations to the soliton field owing to changes in photon number, phase, momentum (frequency), and position (time), respectively, whereas f_c and f_s represent amplitude and phase perturbations of the continuum, respectively. The equations of motion for the operator coefficients are found by substitution of the modal expansion into the linearized nonlinear Schrödinger equation and employment of the orthogonality relations described in Refs. 5 and 6. In this way the inverse Fourier transforms of the correlators in Eqs. (5)–(7), in their unordered form, are shown to be

$$G^{cc}(\tau, \tau', \xi) = 4\sum_{i,j=n,p,c} \langle\Delta\hat{X}_i(\tau)\Delta\hat{X}_j(\tau')\rangle_\xi, \tag{10}$$

$$G^{ss}(\tau, \tau', \xi) = 4\sum_{i,j=\theta,\tau,s} \langle\Delta\hat{X}_i(\tau)\Delta\hat{X}_j(\tau')\rangle_\xi, \tag{11}$$

$$G^{cs}(\tau, \tau', \xi) = 4\sum_{i=n,p,c;\,j=\theta,\tau,s} \langle\Delta\hat{X}_i(\tau)\Delta\hat{X}_j(\tau')\rangle_\xi. \tag{12}$$

We evaluated all the second-order moments between the operator coefficients that are present in Eqs. (10)–(12) for arbitrary values of ξ. Defining $\alpha \equiv (1 + \Omega^2)\xi/2$, $\beta \equiv (\Omega^2 - \Omega'^2)\xi/2$, and $\gamma \equiv (2 + \Omega^2 + \Omega'^2)\xi/2$, we obtain the following nonzero moments:

$$\langle\hat{V}_n^2\rangle_\xi = 1/2, \quad \langle\hat{V}_\theta^2\rangle_\xi = (\pi^2 + 12)/72 + \xi^2/2, \tag{13}$$

$$\langle\hat{V}_p^2\rangle_\xi = 1/6, \quad \langle\hat{V}_\tau^2\rangle_\xi = (\pi^2 + 4\xi^2)/24, \tag{14}$$

$$\begin{bmatrix} \langle\hat{V}_n\hat{V}_\theta\rangle_\xi \\ \langle\hat{V}_p\hat{V}_\tau\rangle_\xi \end{bmatrix} = \frac{i}{4}\begin{bmatrix} -1 \\ 1 \end{bmatrix} - \xi\begin{bmatrix} 1/2 \\ 1/6 \end{bmatrix}, \tag{15}$$

$$\begin{bmatrix} \langle\hat{V}_n\hat{V}_c(\Omega)\rangle_\xi \\ \langle\hat{V}_n\hat{V}_s(\Omega)\rangle_\xi \\ \langle\hat{V}_p\hat{V}_c(\Omega)\rangle_\xi \\ \langle\hat{V}_p\hat{V}_s(\Omega)\rangle_\xi \end{bmatrix} = \frac{a_0(\Omega)}{4}\begin{bmatrix} -\cos\alpha \\ \sin\alpha \\ (\Omega/3)\cos\alpha \\ -(\Omega/3)\sin\alpha \end{bmatrix}, \tag{16}$$

$$\begin{bmatrix} \langle\hat{V}_\theta\hat{V}_c(\Omega)\rangle_\xi & \langle\hat{V}_\tau\hat{V}_c(\Omega)\rangle_\xi \\ \langle\hat{V}_\theta\hat{V}_s(\Omega)\rangle_\xi & \langle\hat{V}_\tau\hat{V}_s(\Omega)\rangle_\xi \end{bmatrix} = \begin{bmatrix} \sin\alpha & -\xi\cos\alpha \\ \cos\alpha & \xi\sin\alpha \end{bmatrix}$$
$$\times\begin{bmatrix} \langle\hat{V}_\theta\hat{V}_s(\Omega)\rangle_0 & \langle\hat{V}_\tau\hat{V}_s(\Omega)\rangle_0 \\ \langle\hat{V}_n\hat{V}_c(\Omega)\rangle_0 & \langle\hat{V}_p\hat{V}_c(\Omega)\rangle_0 \end{bmatrix}, \tag{17}$$

$$\begin{bmatrix} \langle\hat{V}_c(\Omega)\hat{V}_c(\Omega')\rangle_\xi \\ \langle\hat{V}_s(\Omega)\hat{V}_s(\Omega')\rangle_\xi \\ \langle\hat{V}_c(\Omega)\hat{V}_s(\Omega')\rangle_\xi \end{bmatrix} = \begin{bmatrix} 1 & \cos\beta & -\cos\gamma \\ 1 & \cos\beta & \cos\gamma \\ i & \sin\beta & \sin\gamma \end{bmatrix}$$
$$\times\frac{\pi}{2}\begin{bmatrix} \delta(\Omega - \Omega') \\ \dfrac{(\Omega - \Omega')^2 + 4}{6(\Omega^2 + 1)(\Omega'^2 + 1)}\dfrac{(\Omega - \Omega')}{\sinh[\pi(\Omega - \Omega')/2]} \\ \dfrac{(\Omega + \Omega')^2 - 6\Omega\Omega' - 2}{6(\Omega^2 + 1)(\Omega'^2 + 1)}\dfrac{(\Omega + \Omega')}{\sinh[\pi(\Omega + \Omega')/2]} \end{bmatrix}, \tag{18}$$

$$\langle\hat{V}_\theta\hat{V}_s(\Omega)\rangle_0 = -\frac{a_0(\Omega)}{4}\left[\frac{2/3}{\Omega^2 + 1} + \frac{\pi\Omega}{6}\tanh\left(\frac{\pi\Omega}{2}\right)\right], \tag{19}$$

$$\langle\hat{V}_\tau\hat{V}_s(\Omega)\rangle_0 = \frac{a_0(\Omega)}{2}\left[\frac{\Omega}{\Omega^2 + 1} - \frac{\pi}{4}\tanh\left(\frac{\pi\Omega}{2}\right)\right]. \tag{20}$$

Note that all the operator coefficients of the same class (i.e., cosine or sine) commute with each other.

We evaluated the integrals that are present in Eqs. (10)–(12) numerically, took the Fourier transforms of the resulting correlators, and used them in Eq. (4) to obtain the Fano factor. The results are plotted in Fig. 1 versus the intensity-transmission coefficient T and the propagation distance $z \equiv 2\xi/\pi$ in soliton periods. As shown, large amounts of squeezing can be obtained for propagation distances $z > 3$. The
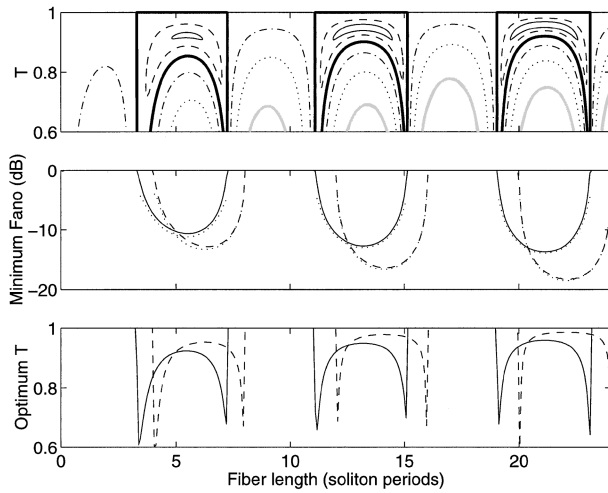
Fig. 1.   Top: contour plot showing the Fano factor, including dispersion, versus T (solid curves, $F = -10$ dB; dashed curves, $F = -5$ dB; thick solid curves, $F = 0$ dB; dotted-dashed curves, $F = 5$ dB; dotted curves, $F = 10$ dB; thick gray curves, $F = 15$ dB).   Middle: Fano factor minimized by the proper choice of T with (solid curves) and without (dashed curves) dispersion taken into account; the Fano factor limit imposed by the loss $(1 - T)$ in each case (dotted curves) is also shown.   Bottom: optimum T corresponding to the minimum Fano factor in the middle figure, with (solid curves) and without (dashed curves) dispersion.   The distance is in soliton periods in all three plots.

noise-reduction regions repeat approximately every eight soliton periods; propagation over this distance results in the soliton's acquiring a nonlinear phase shift $\Delta \xi/2 = 2\pi$ with respect to the weak pulse.   The first three local minima of the Fano factor are found to be -10.6 dB ($z \approx 5.5$, $T \approx 0.92$), -12.7 dB ($z \approx 13.2$, $T \approx 0.95$), and -13.7 dB ($z \approx 21.1$, $T \approx 0.96$).

The periodicity in the Fano factor indicates that the physical mechanism behind the noise reduction in a Sagnac interferometer is very similar to those of the cw field in a nonlinear Mach–Zehnder interferometer[7] and of soliton quadrature squeezing.[5]   As the soliton propagates in one direction around the loop, one of the field quadratures becomes squeezed owing to self-phase modulation.   This squeezing is manifested by the correlations of $\hat{V}_n$, $\hat{V}_c$, with $\hat{V}_\theta$, $\hat{V}_s$.   Although the amount of squeezing increases with ξ, the angle of the squeezed quadrature with respect to the soliton mean field approaches zero.   The amplitude quardrature, however, remains unsqueezed.   By mixing a small coherent mean-field component with the squeezed soliton field, one can rotate the output mean field a_{out} to select the minimum noise quadrature[7,8] while introducing only a small amount of loss to the squeezed component.   The Sagnac interferometer performs the mixing of the two fields with the relative phase shift determined by the nonlinear phase of the soliton inside the fiber loop.   This configuration provides good stability of the interference while limiting the minimum Fano factor by only the amount of the beam-splitter loss, $1 - T$.   To illustrate this point we calculated the optimum noise reduction for the case in which the dispersion in the weaker pulse is turned off [ψ in Eq. (2) is set

to 0].   In Fig. 1 we compare the Fano factors with and without dispersion in the weaker pulse with the limits set by the corresponding beam-splitting losses, $1 - T$.   One can see that the amount of available quadrature squeezing inside the loop is large enough to make $1 - T$ the main constraint on the observable noise reduction.   For long propagation distances the fundamental soliton $a_0(\tau) = \text{sech}(\tau)$ is close to the matched local-oscillator shape for detection of quadrature squeezing.[5]   Therefore, since the undispersed pulse is better matched to the squeezed mode than is the dispersed pulse, the amount of mean field needed to rotate the output field is smaller, resulting in lower necessary loss, $1 - T$.   As z increases, the optimum transmission approaches unity, and the Fano factor becomes arbitrarily small in an increasingly narrow range of values of T.   On the other hand, when the dispersion of the weaker pulse is taken into account, the optimum transmission becomes smaller and the requirement on its tolerance relaxes, whereas the achievable noise reduction suffers.   For longer propagation distances (up to $z = 50$), we find that the Fano factor slowly approaches a value of $F \approx -16$ dB.   Note that in the time domain dispersion also leads to a mean phase shift of a_{gvd} with respect to a_{sol}, causing regions of optimum squeezing to slide toward shorter z by approximately one soliton period.

Although our model does not provide numerical estimates when the pulse propagating in the strong arm of the interferometer is not a soliton ($N \neq 1$), one can make approximate predictions by shifting the ranges of squeezing in Fig. 1 along the z direction by the amount of the additional nonlinear phase shift.   Such predictions are found to be in agreement with numerical[1,3] and experimental[3,4] results.

References

1. M. J. Werner, presented at the OSA Annual Meeting, October 11–17, Long Beach, California, 1997; M. J. Werner and S. R. Friberg, in *International Quantum Electronics Conference*, Vol. 7 of 1998 OSA Technical Digest Series (Optical Society of America, Washington, D.C., 1998), p. 130.
2. S. J. Carter, P. D. Drummond, M. D. Reid, and R. M. Shelby, Phys. Rev. Lett. **58,** 1841 (1987).
3. S. Schmitt, J. Ficker, M. Wolff, F. Köenig, A. Sizmann, and G. Leuchs, Phys. Rev. Lett. **81,** 2446 (1998).
4. D. Krylov and K. Bergman, Opt. Lett. **23,** 1390 (1998).
5. H. A. Haus and Y. Lai, J. Opt. Soc. Am. B **9,** 386 (1990); H. A. Haus, W. S. Wong, and F. I. Khatri, J. Opt. Soc. Am. B **14,** 304 (1997).
6. D. Levandovsky, M. Vasilyev, and P. Kumar, Opt. Lett. **24,** 43 (1999).
7. M. Kitagawa and Y. Yamamoto, Phys. Rev. A **34,** 3974 (1986).
8. M. Margalit, E. P. Ippen, and H. A. Haus, in *International Quantum Electronics Conference*, Vol. 7 of 1998 OSA Technical Digest Series (Optical Society of America, Washington, D.C., 1998), p. 170.